Review Article

Shigeru Ikeda*

Copper-based kesterite thin films for photoelectrochemical water splitting

https://doi.org/10.1515/htmp-2021-0050
received September 24, 2021; accepted December 08, 2021

Abstract: Copper kesterite Cu_2ZnSnS_4 is a promising photoabsorber material for solar cells and photoelectrochemical (PEC) water splitting. In this article, we will first review the crystallographic/energetic structures of Cu_2ZnSnS_4 in view of its applications to sunlight conversion devices. Then, historical progress in photovoltaic properties of Cu_2ZnSnS_4-based solar cells is introduced. Finally, studies on PEC H_2 evolution over Cu_2ZnSnS_4-based photocathodes are reviewed in detail. For realizing efficient PEC H_2 evolution, surface modifications with an n-type buffer layer (such as CdS) and a catalytic site (such as Pt nanoparticles) were found to be indispensable. Since these surface-modified photocathodes had poor resistances under an operating bias due to the occurrence of oxidative photocorrosion of the CdS layer and elimination of the Pt catalysts, coverage with a protection layer was required to improve the long-term durability. Moreover, partial or complete substitution of the constituent cations with some cations was proved to be effective for improving PEC properties. Although recent studies showed a rapid increase in PEC properties, there is room for further development of PEC properties by using effective combinations among surface protection(s), defect engineering(s), and band engineering(s).

Keywords: photoelectrochemical water splitting, photocathode, copper kesterite thin films

1 Introduction

The energy problem is one of the most important technological problems faced by the world. Current world power consumption is estimated to be ca. 19 TW, more than 80% of which is generated from fossil fuels [1]. Since mankind's demand for energy is already causing climate changes that might lead to serious long-term consequences for the earth, transfer of the global energy supply system to a renewable energy source is an urgent issue. Among the various kinds of renewable energy resources, sunlight has attracted much attention due to its abundancy and permanency. Based on the solar constant (1366.1 $W \cdot m^{-2}$), the total solar flux reaching the earth's surface is estimated to be ca. 180,000 TW. When absorption and scattering are considered (i.e., assumption of 50% loss), the actual value would be 90,000 TW, indicating that ca. 0.02% of solar energy is equivalent to the energy demand by human society. Hence, part of the solution to the energy problem must come from increased exploitation of solar energy. Current practical systems of widespread deployments are based on solar cells; several energy conversion facilities with a scale of several hundred GW have been installed throughout the world [2]. However, these sunlight-based systems require several costly devices not only for sunlight-to-electricity conversion (solar cells) but also for storage and transportation.

A solution to avoid the cost issue is solar-to-fuel conversion, in which light energy in sunlight is converted into chemical energy in the form of gas or liquid fuels [3]. Instead of an expensive battery, fuels can be stored in a simple tank or pool without a natural discharge phenomenon. Moreover, fuels are transportable by using conventional tankers and pipelines. Among the many kinds of fuels, hydrogen (H_2) is an attractive fuel because of its relatively high energy density per weight (120 $MJ \cdot kg^{-1}$) and the possibility of construction of a carbon-free substance circulation system [4]. To realize solar-to-hydrogen conversion, one of the most probable methods consisting of a combination of current conventional technologies is water electrolysis into H_2 and oxygen (O_2) in conjunction with the electricity generated by solar cells. However, the process cost of the wiring over each cell as well as the necessity of a water electrolyzer including costly electrocatalysts makes this type of system expensive compared to its energy conversion efficiency [5].

* **Corresponding author: Shigeru Ikeda,** Department of Chemistry, Konan University, 9-1 Okamoto, Higashinada-Ku, Kobe, Hyogo 658-8501, Japan; Institute for Energy Conversion Materials, Konan University, 9-1 Okamoto, Higashinada-Ku, Kobe, Hyogo 658-6 8501, Japan, e-mail: s-ikeda@konan-u.ac.jp

Use of powdered photocatalysts dispersed in a solution or embedded onto a monolithic sheet is expected to become the most scalable and cost-effective device because of their simplicity [6,7]. The photocatalytic reaction is directly driven on the surface of the semiconductor by electrons and holes generated by a photoexcitation process. Since the surfaces of semiconductor powders are often inert to induce water splitting reactions, loading(s) of co-catalyst(s) for H_2 and/or O_2 evolution are introduced on their surfaces. The first demonstration of direct photocatalytic overall water splitting was reported in 1980s by using a $SrTiO_3$ powder-based photocatalyst: $SrTiO_3$ powder modified with NiO_x, a catalyst for H_2 evolution [8]. However, since the photocatalyst could only utilize ultraviolet light with low photocatalytic activity, the development of visible-light-responsive photocatalyst with high activity has been investigated in order to achieve meaningful solar to hydrogen efficiencies (STHs). As a result, several photocatalyst materials including GaN:ZnO [9], $LaMg_{1/3}Ta_{2/3}O_2N$ [10], and $Y_2Ti_2O_5S_2$ [11] have been found to be active for overall water splitting reaction under visible light irradiation. A photocatalytic reaction system using a two-step photoexcitation process is often called a Z-scheme photocatalytic system [12–15]. The system consists of two photocatalysts: one photocatalyst induces water reduction into H_2 and the other produces O_2 by water oxidation on its surface. Many kinds of photocatalysts have been shown to be applicable for the system. As a recent example, a photocatalyst sheet in which $SrTiO_3$:La,Rh and $BiVO_4$:Mo powders are embedded showed a high STH value (1.2%) [16]. Since both the single photocatalyst system and Z-scheme system generate a mixture of H_2 and O_2 gases with a compositional ratio of 2:1, so-called oxyhydrogen detonation gas, installation of an additional separation system such as a separation membrane is required [17]. This is one of the most critical problems of these particulate photocatalyst-based systems for their practical use.

Another promising system using the two-step photoexcitation process is a photoelectrochemical (PEC) cell in which two kinds of semiconductor electrodes, photocathode and photoanode for H_2 and O_2 evolutions, respectively, are used (Figure 1) [18–20]. In this system, reaction sites for H_2 and O_2 evolutions are located far away from each other as in a water electrolyzer. Thus, the system does not require a separation process and apparatus for generated H_2 and O_2. Moreover, surface modifications can be applied to each photoelectrode to improve its performances such as charge separation efficiency and stability. For photocathode materials for H_2 evolution, Cu-based selenides and sulfides and their mixed forms of selenosulfides crystallized in a chalcopyrite structure ($Cu(In,Ga)(Se,S)_2$) were shown to be effective upon modifications on their surfaces for inducing water reduction [21–38]. Since pioneering works in the early 2010s [21,22], appreciable improvements have been achieved: the current record STH value for unbiased overall water splitting of 3.7% upon combination with a $BiVO_4$-based photoanode for O_2 evolution was achieved by using a chalcopyrite $Cu(In,Ga)Se_2$-based photocathode [34]. However, due to the low abundance of constituent elements (i.e., In, Ga, and Se), these chalcopyrite compounds are unlikely to be sustainable in the long term for large-scale developments. A promising candidate for a sustainable photocathode material is copper zinc tin sulfide (Cu_2ZnSnS_4, commonly known as CZTS) since it has electric properties similar to those of $Cu(In,Ga)Se_2$, but contains cheap and plentiful less-toxic elements. In this review, therefore, we focus on CZTS and related compounds for their applications as photocathodes for PEC H_2 evolution under sunlight irradiation. Following the description of several fundamental

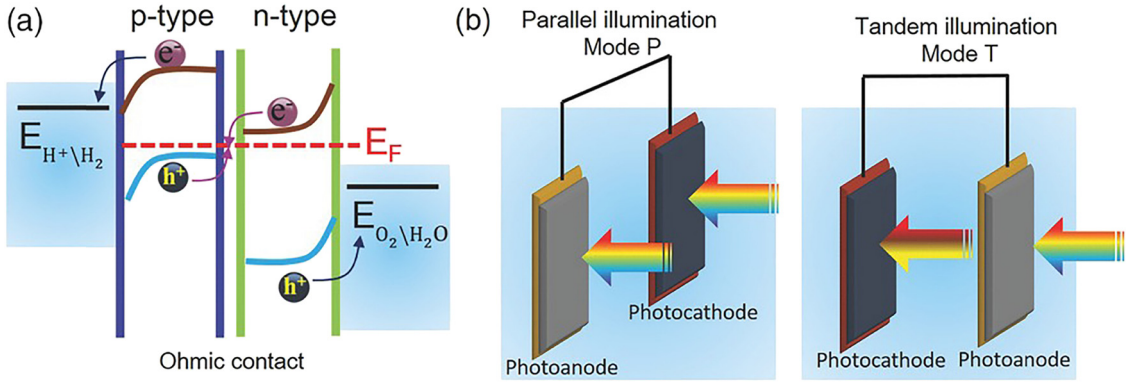

Figure 1: (a) Working principle of a PEC cell for overall water splitting based on a photoanode and a photocathode in a tandem configuration. (b) A schematic of the wired PEC tandem cell under a parallel (left) and a tandem (right) illumination. Reprinted with permission from ref. [20]. ©2016 Wiley-VCH.

aspects of these compounds as well as the operating principle of PEC water splitting, the history of development of CZTS-based photocathodes is overviewed with focus on the surface modifications and substitutions of constituent elements to improve PEC H_2 evolution properties.

2 Crystallographic and energetic structures of CZTS

The CZTS crystal is derived from the zinc-blende structure of II–VI semiconductors such as ZnS. By substituting half of the group II element with a group I element (e.g., Cu) and half with a group III element (e.g., In), a I–III–VI_2 compound semiconductor crystalized in a chalcopyrite structure (i.e., $CuInS_2$) can be formed. Further substitution of the group III element of In with half of a group II element (e.g., Zn) and half of a group IV element (e.g., Sn) will result in a I_2–II–IV–VI_4 compound of CZTS. In general, CZTS has two principal structures known as kesterite and stannite structures, as shown in Figure 2 [39]. Both of them are tetragonal structures that consist of a cubic close packing array of sulfur anions and half of tetrahedral voids of cations. The difference of these two structures is the arrangement of Cu and Zn atoms: the kesterite structure is an ordered array of (Cu,Sn), Se, (Cu,Zn), Se,... layers along the *c*-axis, whereas the stannite structure is an ordered array of (Zn,Sn), Se, Cu, Se,... layers along the *c*-axis. Since Cu^+ and Zn^{2+} cations have identical number of electrons, it is difficult to determine their positions in the unit cell by conventional X-ray diffraction. However, the CZTS crystal has been considered to appear in the kesterite phase because of its relatively high levels of thermodynamical stability compared to that of the stannite phase [40]. A structural investigation of a powdered CZTS sample using neutron diffraction also indicated crystallization of the kesterite structure [41].

The kesterite CZTS has a band gap (E_g) of 1.5 eV. The origin of the conduction band minimum (CBM) is mainly attributed to the s orbital of Sn (Sn-5s) and s, p orbitals of S (S-3s, S-3p), whereas the valance band maximum (VBM) is derived from the d orbital of Cu (Cu-3d) and the p orbital of S (S-3p) [39,42]. These electron energy structures of CZTS suggest possible engineering of band edge potentials by partial and/or complete substitutions of constituent elements. In most of the works on the solar cell application, partial substitution of S with Se to form a sulfoselenide (CZTSSe) has been studied [43–48]. With higher Se content (i.e., lower S/(S + Se) ratios), the CBM shifts downward, while the VBM shifts upward, resulting in possible controls of band gap energies (E_gs) ranging from 1.0 eV (pure selenide CZTSe) to 1.5 eV (pure sulfide CZTS) by changing the S/(S + Se) ratio, as shown in Figure 3 [49,50]. Both the experimental and theoretical investigations indicated that these copper kesterites have a large band-edge absorption coefficient $>10^4$ cm^{-1} as similar to that of copper chalcopyrite compounds [49,51]. Moreover, as is well known for copper chalcopyrite compounds [52], replacements of cation components are also effective for modifying E_g, VBM, and CBM energies. Examples for these cation substitutions for band engineering of CZTS are discussed below.

Conversion of elemental precursors into the CZTS quaternary compound takes place in competition with the formation of other secondary phases such as Cu_2S, SnS_2, Cu_2SnS_3, and ZnS. A comprehensive analysis of the Cu_2S–ZnS–SnS_2 pseudoternary system at 400°C carried out by Olekseyuk et al. indicated that a CZTS single

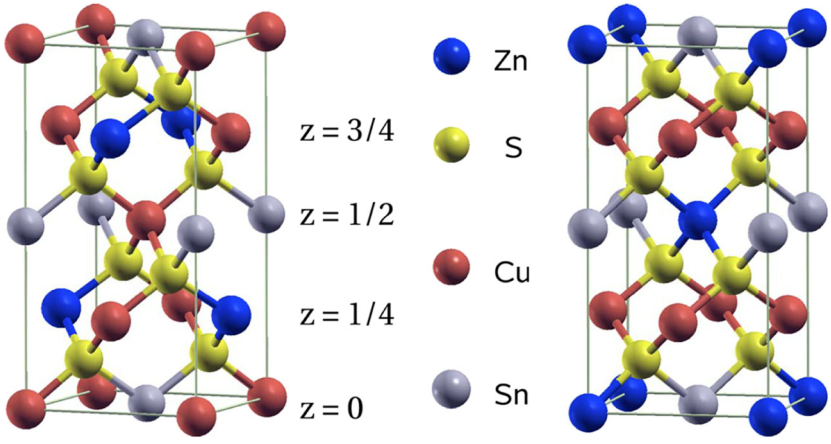

Figure 2: Kesterite (left) and stannite (right) structures of CZTS material. Reprinted with permission from ref. [39]. ©2009 American Physical Society.

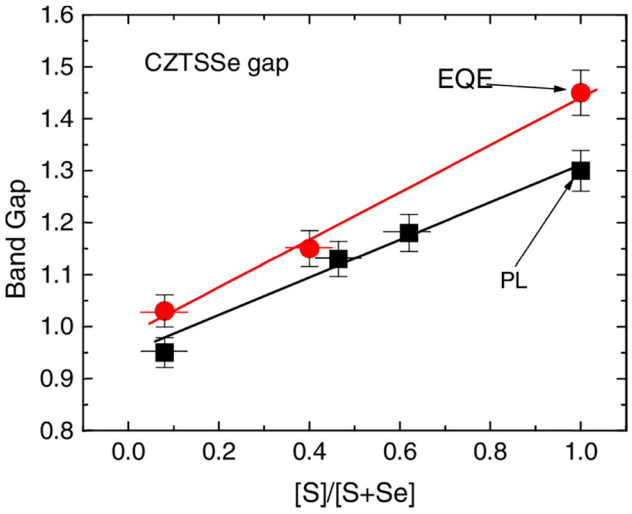

Figure 3: E_gs of CZTSSe as a function of (S)/(S + Se) derived from photoluminescence (PL) (solid squares) and from external quantum efficiency EQE (solid circles). Reprinted with permission from ref. [50]. ©2011 AIP Publishing.

phase is present only within a small region [53]. Theoretical analysis of the formation window of CZTS in a Cu_2S–ZnS–SnS_2 pseudoternary system also suggested the similar trend, as shown in Figure 4 [54]. There are four two-phase fields in which one secondary phase, i.e., Cu_2S, Cu_2SnS_3, SnS_2, or ZnS, will be observed in addition to CZTS. Between them, four phase fields, where the secondary phase from the bordering fields will be formed together with CZTS, are present. From a study in the photovoltaic field, the Cu_2S compound is known to be highly doped p-type, leading to the generation of a shunt current flow in a solar cell [55], Cu_2SnS_3 is p-type having moderate E_g (1–1.35 eV) but is inefficient as a photoabsorber [56,57]. Since SnS_2 is an n-type compound, inclusion of this phase would form a secondary diode inside the CZTS film, resulting in enhancement of carrier recombination [55,58]. ZnS is insulated with E_g of 3.5 eV: it is normally silent in the solar cell compared to the other abovementioned secondary phases, though a high content of ZnS should induce reduction in the active area and increase in resistivity. An empirically optimum composition of the elemental precursor of CZTS as a photoabsorber in a solar cell is a Zn-rich and Cu-poor composition to optimize suppression of the abovementioned harmful secondary phases except for the silent ZnS phase and formation of Cu vacancy (V_{Cu}), a favorable p-type point defect.

Due to the quaternary nature, there are many types of intrinsic point defects in CZTS such as vacancies, antisites, and interstitials. Table 1 summarizes the probable point defects formed in CZTS and their calculated formation energy; corresponding energy levels are shown in Figure 5 [59,60]. To realize efficient utilization of photoexcited carriers for energy of a useful form such as electricity or fuel, it is critically important to obtain a systematic understanding of the characteristics of these defect properties that determine the level of self-doping as well as the rate of nonradiative recombination of photoexcited carriers. In chalcopyrite $CuInSe_2$, it is well known that p-type self-doping is due to the Cu vacancy (V_{Cu}) [61,62]. For the CZTS compound, a theoretical calculation indicated that the Cu on Zn antisite (Cu_{Zn}) and V_{Cu} are dominant acceptor point defects that lead to

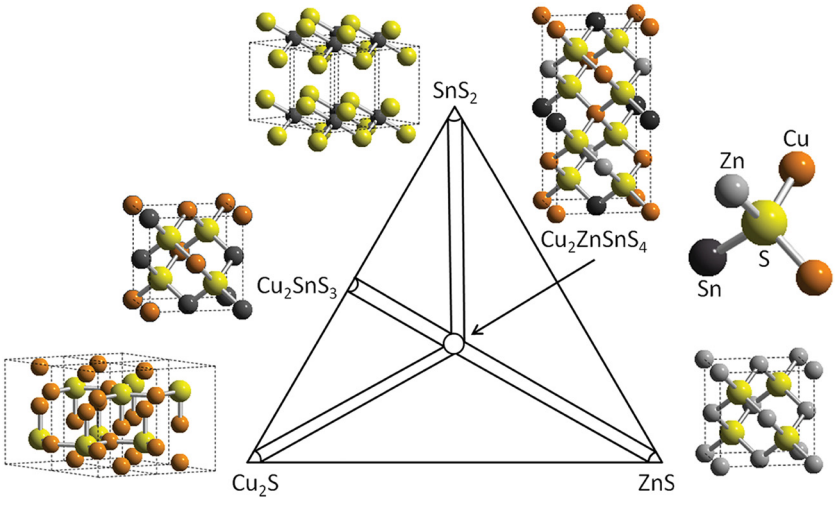

Figure 4: Schematic of a thin-film Cu_2S–ZnS–SnS_2 ternary phase diagram at a deposition temperature of 325°C. Reprinted with permission from ref. [54]. ©2011 AIP Publishing.

Table 1: Formation energies of point defects in CZTS determined by theoretical calculations [59]

Type	Symbol	Formation energy[1] (eV)	Electrical property
Vacancy	V_{Cu}	0.67	Acceptor
Vacancy	V_{Zn}	1.02	Acceptor
Vacancy	V_{Sn}	2.72	Acceptor
Antisite	Cu_{Zn}	0.01	Acceptor
Antisite	Zn_{Cu}	2.43	Donor
Antisite	Cu_{Sn}	0.87	Acceptor
Antisite	Sn_{Cu}	6.54	Donor
Antisite	Zn_{Sn}	0.69	Acceptor
Antisite	Sn_{Zn}	4.11	Donor
Interstitial	Cu_i	3.23	Donor
Interstitial	Zn_i	6.02	Donor
Interstitial	Sn_i	8.22	Donor
Vacancy	V_S	1.09	Donor

[1] Formation energies were extracted from the data given in ref. [59] for the case of a stable Cu-poor region of pure CZTS crystal.

p-type conductivity [59,60]. Cu_{Zn} has lower formation energy than that of V_{Cu} and an acceptor energy level of 0.12 eV above the VBM. Since V_{Cu} has relatively low acceptor energy level (0.02 eV above the VBM), V_{Cu} is the most preferable point defect in CZTS. Nagaoka et al. reported that electrical properties examined by using a high quality CZTS single crystal obtained by traveling heater method, a solution growth technique, with a Zn-rich and Cu-poor composition [63] revealed that native acceptors in CZTS have a larger activation energy than that of a copper chalcopyrite ($Cu(In,Ga)Se_2$) single crystal, indicating that relatively deep level, i.e., Cu_{Zn} is the main exiting point defect in the CZTS single crystal [64]. Although, the CZTS thin films used for solar cells and PEC water splitting were obtained in a non-equilibrium state, these theoretical and experimental results suggest that Cu_{Zn} exits in the CZTS films at a higher concentration than that of V_{Cu}. Due to the deeper energy level of Cu_{Zn} than that of V_{Cu}, the existence of a high concentration of Cu_{Zn} leads to enhancement of fluctuation and band tailing [65,66] and reduction in band bending (built-in potential) [67]. Therefore, a successful combination of suppression of the formation of Cu_{Zn} and increment in V_{Cu} in the CZTS crystal should be promising to improve efficiencies of CZTS-based devices for photon energy conversion. Doping of a secondary element for substituting constituents is a possible option to realize such a point defect engineering. Several applications of this concept for a PEC H_2 evolution device will be described later.

3 CZTS thin-film solar cells

The potential of the CZTS compound for use in solar cells was first reported by Ito and Nakazawa in 1988 [51]. They prepared CZTS thin films by atom beam sputtering and made a device with a cadmium tin oxide transparent conductive layer. The thus-obtained device showed an open circuit voltage (V_{OC}) of 165 mV under simulated sunlight (AM 1.5G) illumination. After their findings, many efforts were made to develop thin-film solar cells using CZTS as an absorber layer. In 1996, Katagiri et al. reported successful fabrication of CZTS thin films by sulfurization of electron beam (EB)-evaporated precursor [68]. They constructed a solar cell with a structure of Al/ZnO/CdS/CZTS/Mo/glass and achieved an appreciable sunlight conversion efficiency (η) of 0.66% for the first time. In 1997,

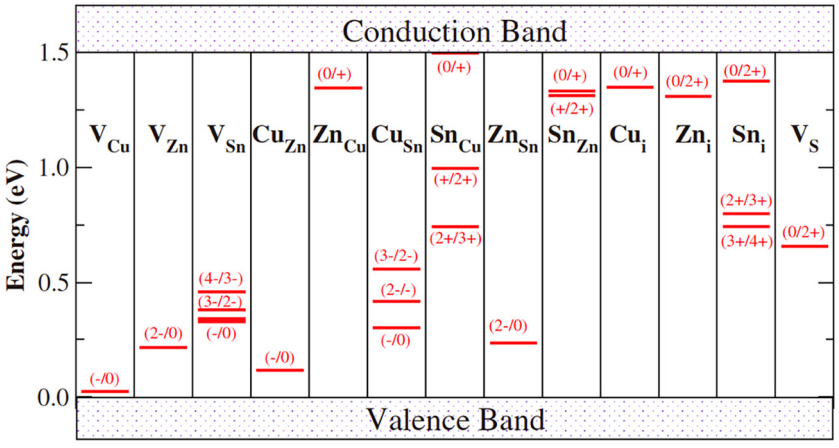

Figure 5: Transition-energy levels of point defects in the E_g of CZTS. Reprinted with permission from ref. [59]. ©2010 American Physical Society.

Friedlmeier et al. fabricated CZTS thin films using thermal evaporation of the elements and binary chalcogenides in high vacuum: a solar cell based on the thus-obtained CZTS film with a structure of CZTS/CdS/ZnO showed η of 2.3% [69]. In 1999, Katagiri et al. produced a CZTS solar cell with η of 2.63% using CZTS thin films, which were fabricated from a Cu–Sn–ZnS stack precursor layer deposited by using EB evaporation followed by sulfurization in an N_2-diluted H_2S atmosphere [70]. That group also improved η to 5.45% in 2003 and to 6.7% in 2008 by optimization of the sulfurization process [71]. Rapid improvements in solar cell properties were demonstrated in 2010–2014 by applying a sulfoselenide CZTSSe as a photoabsorber instead of CZTS [43–45]. Initially, Todorov et al. reported a conversion efficiency of solar cells of 9.6% by using a CZTSSe absorber layer deposited by spin coating using a hydrazine-based precursor solution containing metal binary chalcogenides followed by sulfurization or selenization [43]. The conversion efficiency was then improved up to 12.6% in 2014 [45]. Recently, Gong et al. achieved a record update of the sulfoselenide-based device to η of 13.0% [48]. Regarding a pure sulfide CZTS-based device, Yan et al. broke the record: η of 11.5% was achieved by applying partial replacement of the Zn component in CZTS with Cd [72]. The concept of substitution of constituent cations in CZTS was also applied for a PEC device, the details of which are discussed in Section 6.

4 Operation of PEC water splitting

Semiconductor–redox electrolyte contact is characterized by equilibration of the semiconductor Fermi level with the redox potential of the solution, resulting in the formation of a rectifying contact that is the same as that of a Schottky junction for a semiconductor–metal junction (Figure 1). Photogenerated electrons in a photocathode induce reduction of water into H_2 under cathodic polarization, whereas photogenerated positive holes in a photoanode induce oxidation of water into O_2 under anodic polarization. In the case of a PEC cell composed of the combination of a photocathode and a photoanode, the working current, J_{op} (mA·cm^{-2}), is obtained as an intersection point of current–potential curves of the photocathode and photoanode, as shown in Figure 6 [18]. The corresponding potential at the crossing point is called a working potential. Therefore, to achieve a high current density, i.e., a high STH, the photocurrent at the crossing point should be improved. For a PEC cell composed of the combination of photoelectrodes, STH is defined by equation (1):

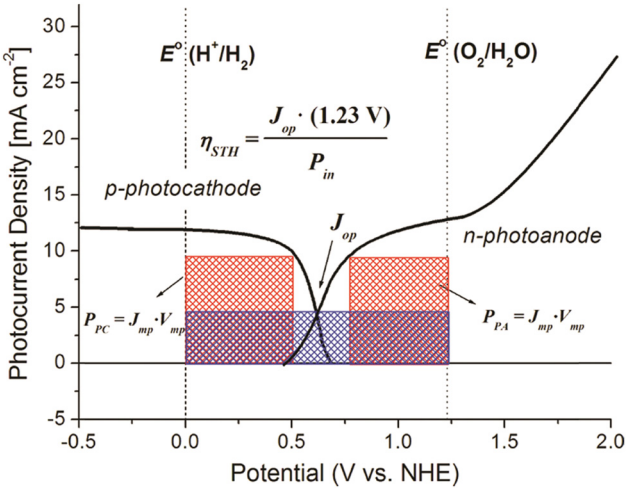

Figure 6: Overlaid current density–potential (J–V) behavior for a p-type photocathode and an n-type photoanode, with overall efficiency generated by the cell for splitting water. Reprinted with permission from ref. [18]. ©2010 American Chemical Society (ACS).

$$\mathrm{STH}(\%) = [(1.23 \times J_{\mathrm{op}})/P] \times 100, \quad (1)$$

where P is the energy of incident sunlight, the value of which is usually 100 mW·cm^{-2} corresponding to the ASTM International established standard of sunlight spectra (AM 1.5G). It is clear for the photocathode side that realizing a large photocurrent at a relatively positive potential is directly linked to the achievement of high STH.

Deposition of an additional n-type layer over a p-type photocathode increases the charge separation efficiency through formation of a hetero-type p–n junction. Although the lattice mismatch between the two layers should be considered to suppress formation of interfacial defects, a critical carrier recombination center, this leads to an increased photocurrent and onset potential. Metal sulfide materials such as CdS with a thickness in a scale of several tens of nanometers deposited by the chemical bath deposition (CBD) method have been reported as good surface modifiers for various p-type photocathodes. Although the CBD method limits the choice of available materials, the process has a merit in terms of film conformality, process simplicity, easiness of thickness control, etching effect onto impurity phases, and possible operation in mild conditions. A CdS-based heterojunctin obtained by the CBD method was originally studied for its application in solar cells. An important parameter in a heterojunction is the band alignment of CBMs between the p-type photoabsorber and n-type buffer layer. Device simulations of solar cells composed of chalcopyrite Cu(In,Ga)Se_2 absorbers with different In/(In + Ga) ratios (having different CBM energies) and n-type buffer layers with various CBM energies revealed that a spike-type alignment, i.e., the Cu

$(In,Ga)Se_2$ absorber, with its offset energy (ΔE_C) of 0–0.4 eV is favorable, while a cliff-type alignment with $\Delta E_C < 0$ is unfavorable because it induces an increase in the probability of carrier recombination at the p–n heterointerface, leading to reduction in V_{OC} (Figure 7) [70–73]. For PEC H_2 evolution, the energetic property of p–n heterointerfaces should affect the photocurrent onset. Therefore, as described in the next paragraph, the optimum choice of an n-type buffer material is an important issue for achieving high PEC H_2 evolution properties.

As the first example for the use of a CBD-derived CdS layer in a PEC H_2 evolution system, Yokoyama et al. reported a chalcopyrite $Cu(In,Ga)Se_2$-based photocathode [21]. In their study, the surface of $Cu(In,Ga)Se_2$ was modified with a CdS layer followed by deposition of Pt nanoparticles on the surface of the CdS layer (Pt/CdS/$Cu(In,Ga)Se_2$). As shown in Figure 8, a current density–potential (J–V) plot of the Pt/CdS/$Cu(In,Ga)Se_2$ photocathode measured in an aqueous solution of 0.1 M Na_2SO_4 with pH adjusted to 9.5 indicated 3 times larger photocurrent with a 0.3 V higher onset potential than that obtained by platinized $Cu(In,Ga)Se_2$ without having a CdS buffer layer (Pt/$Cu(In,Ga)Se_2$). In that same period, we investigated PEC H_2 evolution by using a chalcopyrite $CuInS_2$ thin film modified with Pt nanoparticles and we achieved a CdS buffer layer (Pt/CdS/$CuInS_2$) and proved a significant enhancement of PEC H_2 evolution properties by loading of a CBD-derived CdS layer [22]. Moriya et al. performed a semi-quantitative calculation of the built-in electric field of electrolyte-chalcopyrite $CuGaSe_2$ thin film interfaces without and with a CdS buffer layer by using Poisson's equations [23]. They found that the presence of CdS led to an increase in depletion layer width at a certain potential, indicating an enhancement of carrier separation at the interface region of the $CuGaSe_2$ thin film (Figure 9). As another example of an n-type buffer layer, we have demonstrated the effectiveness of a CBD-deposited In_2S_3 buffer layer for a chalcopyrite $CuInS_2$-based photocathode instead of CdS [24]. Spectroscopic evaluation of the CBM offsets of $In_2S_3/CuInS_2$ and $CdS/CuInS_2$ revealed a favorable spike-type positive CBM offset with ΔE_C of 0.27 eV in the $In_2S_3/CuInS_2$ heterojunction, whereas the $CdS/CuInS_2$ junction had an unfavorable cliff-type negative offset of ΔE_C of −0.47 eV (Figure 10), leading to appreciable enhancement of the interface carrier recombination [29].

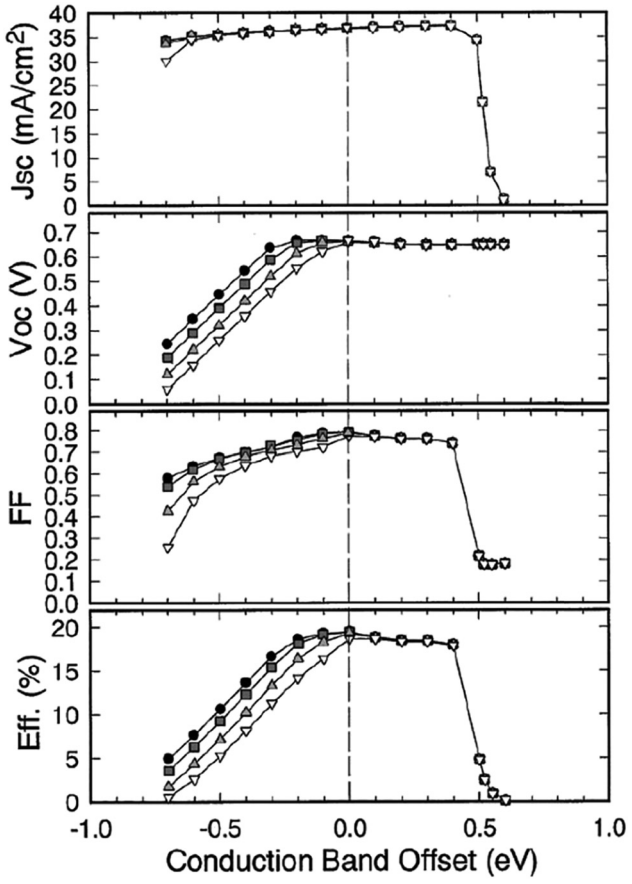

Figure 7: Calculated solar cell parameters as a function of the conduction band offset energy (ΔE_C) between an n-type buffer layer and a $Cu(In,Ga)Se_2$ absorber layer. Reprinted with permission from ref. [73]. ©2001 Elsevier Science B.V.

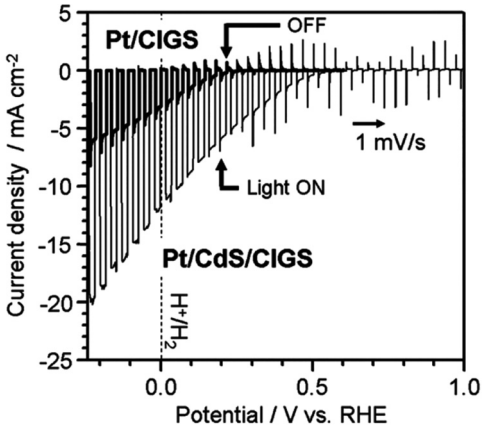

Figure 8: Current density–potential (J–V) plots of Pt/CdS/Cu(In,Ga)Se_2 (Pt/CdS/CIGS) and Pt/$Cu(In,Ga)Se_2$ (Pt/CIGS) photocathodes in 0.1 M Na_2SO_4 aqueous solution (pH = 9.5) under intermittent irradiation of 350–800 nm light. Reprinted with permission from ref. [21]. ©2010 Elsevier Science B.V.

5 CZTS photocathode for PEC H_2 evolution

Table 2 summarizes the existing reports on PEC properties of copper-kesterite-based photocathodes. The first

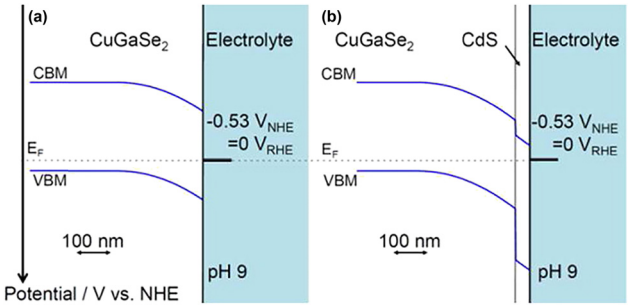

Figure 9: Calculated band alignment at the solid-electrolyte interfaces for (a) $CuGaSe_2$ and (b) CdS/CGSe electrodes. Reprinted with permission from ref. [23]. ©2013 American Chemical Society.

application of CZTS as a photocathode was in 2010 by Yokoyama et al., and a photocurrent density of 2.3 $mA{\cdot}cm^{-2}$ at 0 V_{RHE} was achieved with a CZTS thin film obtained by sulfurization of an EB-deposited Cu/Sn/ZnS precursor layer modified with CdS and Pt nanoparticles [74]. They also reported the effect of loading of a TiO_2 layer between Pt and CdS: the Pt/TiO_2/CdS/CZTS stacked photocathode showed a maximum photocurrent density of 9 $mA{\cdot}cm^{-2}$ at 0 V_{RHE} and a photocurrent onset of 0.6 V_{RHE}. Although details were not discussed, surface-loaded TiO_2 might act as a mediator for electron transfer from the CdS layer to the Pt catalyst. To evaluate a single photocathode under application of external bias voltage, half-cell solar to hydrogen efficiency (HC-STH) was defined by equation (2):

$$\mathrm{STH}(\%) = [(E_{\mathrm{RHE}} \times J_{\mathrm{op}})/P] \times 100, \qquad (2)$$

where E_{RHE} is the working potential referring to a reversible hydrogen electrode (V_{RHE}) [19]. The Pt/TiO_2/CdS/CZTS stacked photocathode achieved the maximum HC-STH of 1.2% at 0.22 V_{RHE}. Improvements in photocurrent density of ca. 12–13 $mA{\cdot}cm^{-2}$ at 0 V_{RHE} and photocurrent onset of 0.85 V_{RHE} were reported by Yang et al. using a Pt/TiO_2/CdS/CZTS stacked photocathode obtained by using a solution-processed CZTS thin film and a TiO_2 layer deposited by an atomic layer deposition (ALD) technique [75].

For the use of a CZTS-based photocathode in a Z-scheme or tandem device, a critical problem of the photocathode modified with a CdS layer and Pt nanoparticles is its poor durability, specifically under applied biases of more than 0 V_{RHE}, i.e., the power generating region. When PEC H_2 evolution is performed at, for example, 0.6 V_{RHE}, the Pt/CdS/CZTS photocathode stack is subjected to oxidative corrosion of CdS layers [30] and delamination of the Pt catalyst [25]. To improve the stability, we found that deposition of a CBD-derived In_2S_3 layer used for the above-described chalcopyrite $CuInS_2$-based photocathode over the surface of the CdS/CZTS stack significantly enhanced its PEC stability [76]. After the deposition of Pt nanoparticles, the photocathode composed of the Pt/In_2S_3/CdS/CZTS stack showed higher durability than that of the photocathode without the In_2S_3 interlayer (Pt/CdS/CZTS). Although the Pt/In_2S_3/CdS/CZTS photocathode was gradually degraded when it used a power generating region, we demonstrated for the first time a successful bias-free overall water splitting by using a CZTS-based photocathode upon combination with $BiVO_4$ (Figure 11). The STH value of the tandem cell was 0.28%.

Further improvements in PEC H_2 evolution properties were also achieved in our subsequent studies by focusing on protection of the CdS layer to suppress its oxidative photocorrosion. In 2018, an HfO_2 ultrathin layer (ca. 6 nm) deposited over the CdS/CZTS stack by ALD was found to be effective as a protection layer [77]. An unbiased solar water splitting device based on the Pt/HfO_2/CdS/

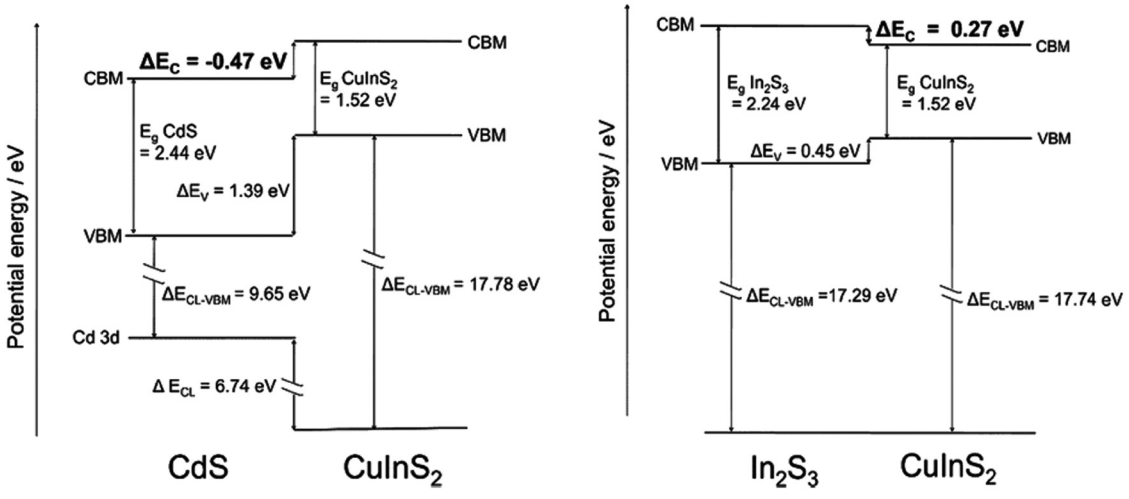

Figure 10: Energy diagrams of CdS/$CuInS_2$ (left) and In_2S_3/$CuInS_2$ (right) heterojunctions estimated from photoabsorption and XP spectroscopy results. Reprinted with permission from ref. [29]. ©2015 American Chemical Society.

Table 2: Properties of copper kesterite photocathodes for water reduction

Year	Photocathode	pH	J_0 (mA·cm^{-1})	Onset (V_{RHE})	HC-STH$_{max}$ (%)	STH (%)	Ref.
2010	Pt–TiO_2/CdS/CZTS	9.5	9.0	0.6	1.2	—	[74]
2015	Pt–In_2S_3/CdS/CZTS	6.5	9.3	0.63	1.63	0.28	[76]
2016	Pt–TiO_2/CdS/CZTS	6.8	12.5	0.85	—	—	[75]
2017	TiO_2/CdS/CBTS	7.0	7.5[1]	0.5[1]	—	—	[83]
2017	Pt–TiO_2/CdS/CBTSSe	4.3	12.08	0.5	1.09	—	[84]
2017	Pt–In_2S_3/CdS/CGZTS	6.5	11.1	0.6	1.7	—	[95]
2018	Pt–HfO_2/CdS/CZTS	6.5	11.9	0.7	2.7[2]	1.046	[77]
2018	Pt–TiMo/CdS/CCZTS	7.0	17.0	0.6	4	—	[80]
2019	Pt–ZnS/CdS/CZTS	6.5	8.0	0.63	2.1	—	[78]
2019	Pt–/CdS/ACZTS	10.0	3.78	0.33	0.32	—	[91]
2020	Pt–/CdS/ACZTS	7.0	17.7	0.85	5.2	—	[92]
2021	Pt–HfO_2/CdS/HfO_2/CZTS	3.0	28.0	0.72	7.27	3.17	[79]
2021	Pt–In_2S_3/CdS/ACZTS	6.5	15.0	0.7	2.4	—	[93]

[1]A 300 W xenon lamp with a UV light cut off filter (less than 420 nm) was used as a light source. [2]The value was obtained after 10 h photoirradiation.

Cu_2ZnSnS_4 photocathode in tandem with a $BiVO_4$ photoanode not only exhibited an STH of more than 1% but also showed high long-term durability of over 10 h (Figure 12). In terms of the application of another CDB-derived n-type layer, ZnS was also found to be effective as a protection layer. Although the photocathode was not proved to have long-term stability, it showed the maximum HC-STH of 2.1% [78]. In our recent study, more than 7% efficient solar water splitting with long-term stability of 24 h was achieved by using an HfO_2/CdS/HfO_2 sandwiched buffer layer [79]. The effect of the deposited HfO_2 ultrathin layer (0.5 nm) by ALD at the CdS/CZTS interface would be suppression of carrier recombination inside the photocathode, whereas the HfO_2 layer (6 nm) between CdS and Pt or the electrolyte was likely to facilitate electron transfer without being trapped. Notable features of the tandem device were its successful increase in size up to 5×5 cm^2: the large device exhibited STH of 3.17% with superior long-term stability over 60 h.

6 Substitution of constituent cations in CZTS to improve PEC performance

As discussed above, the p-type semiconducting properties of CZTS predicted by theoretical studies suggested a critical limitation induced by the presence of CuZn antisite point defects at a high concentration. In the photovoltaic field, substitution of Zn with other cations of larger ionic size is hypothesized to increase the formation energy of Cu_{Zn}. Among the variety of divalent cations, Cd^{2+} proved to be a positive substituent of Zn^{2+}: partial substitution of Zn^{2+} in the crystalline lattice of the CZTS film with Cd^{2+} (CCZTS) induced reduction in Cu_{Zn} (thus leading to reduction in band tailing) as well as increase in grain size, resulting in enhancement of solar cell properties including short circuit current density (J_{SC}), fill factor (FF), and η [68]. Tay et al. applied a CCZTS film fabricated through a solution-processed spin coating to PEC H_2 evolution. As a result, the CCZTS film with a Cd/Zn ratio of 0.67 (i.e., 40% of Zn^{2+} in CZTS being substituted with Cd^{2+}) showed the

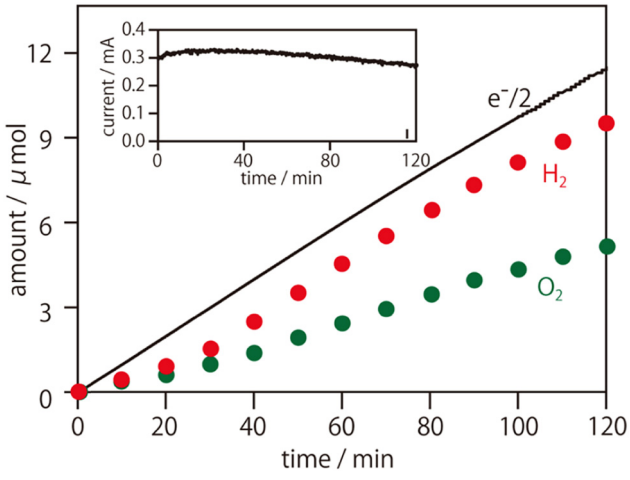

Figure 11: Time course curves of H_2 and O_2 evolution over the Pt/In_2S_3/CdS/CZTS–$BiVO_4$ two-electrode cell under simulated sunlight (AM 1.5G) radiation. The solid line denotes the time course curve of half of the electrons passing through the outer circuit ($e^-/2$). The inset shows the corresponding net current–time curve. Reprinted with permission from ref. [76]. ©2015 American Chemical Society.

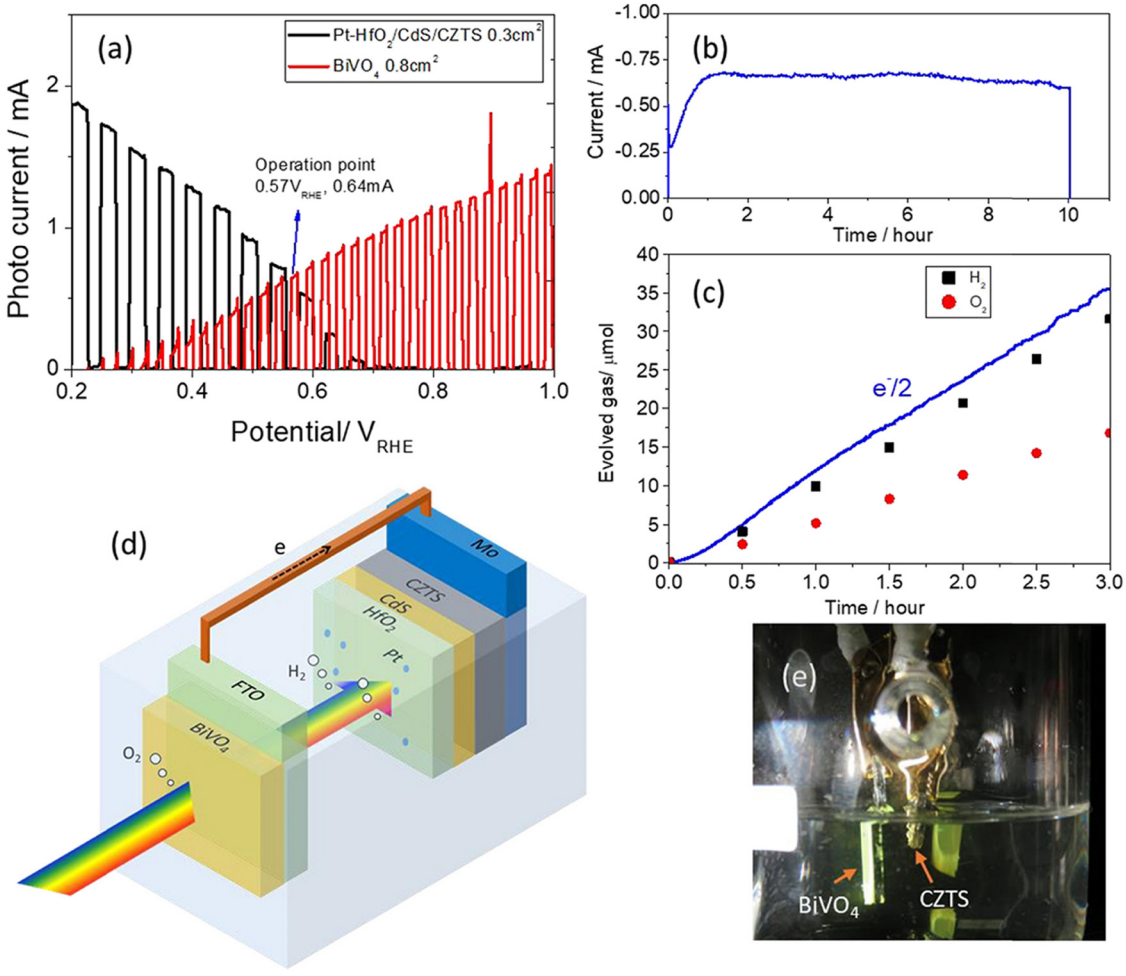

Figure 12: (a) *J–V* curves of a Pt/HfO_2/CdS/Cu_2ZnSnS_4 photocathode and a $BiVO_4$ photoanode under solar simulated AM 1.5G irradiation in a 0.2 mol·dm^{-3} Na_2HPO_4/NaH_2PO_4 solution (pH 6.5). (b) Typical unbiased photocurrent generated from a Pt/HfO_2/CdS/Cu_2ZnSnS_4–$BiVO_4$ tandem device over a 10 h durability test. (c) Time course curves of H_2 and O_2 evolution and $e^-/2$. (d) A picture and (e) a photo of the device. Reprinted with permission from ref. [77]. ©2018 American Chemical Society.

best performance: photocurrent density of the CCZTS-based photocathode at 0 V_{RHE} reached 17.5 mA·cm^{-2} with the maximum HC-STH of 4%, whereas that of a bare CZTS-based photocathode was 5 mA·cm^{-2} at 0 V_{RHE} [80]. As another substituent, Ba^{2+} was also studied not only for PEC H_2 evolution [81–84] but also for photovoltaic application [85,86]. Since Ba adopts much larger coordination due to the large ionic size and its electropositive nature, the formation of detrimental cationic disorders such as CuZn would be suppressed. For the PEC system, for example, substitution of Zn^{2+} in a sulfoselenide CZTSSe thin film with Ba^{2+} (CBTSSe) led to relatively high photocurrent density of more than 12 mA·cm^{-2} at 0 V_{RHE} after applying modifications of its surface with TiO_2/CdS bilayers and Pt nanoparticles [84].

As a similar theory to Cd^{2+} substitution, recent theoretical results reported by Chen et al. predicted that Ag-based kesterite (i.e., Ag_2ZnSnS_4 [AZTS]) has a small number of Ag_{Zn} antisite point defects because significant differences in ionic radii between Ag and Zn ions lead to relatively high formation energy of the defects [87]. Therefore, application of Ag^+ substitution was also studied in photovoltaics [88–90] as well as PEC H_2 evolution [91–93]. It is known that the pure AZTS tends to show an n-type semiconductive characteristic [94]. Thus, in all of the work reported, CZTS films in which Cu^{2+} was partially substituted by Ag^+ with an Ag/(Ag + Cu) ratio up to 0.4 were used. Regarding the PEC performance, actual improvements in the photocurrent density at 0 V_{RHE} were proved. Specifically, a recent work by Tay et al. achieved appreciable improvement in photocurrent density at 0 V_{RHE} (17.7 mA·cm^{-2}) and onset potential of the photocurrent (0.85 V_{RHE}) by using ACZTS photocathodes with an optimum Ag^+ content: the maximum HC-STH

reached 5.2% [92]. As mentioned above for Cd^{2+} substitution, high photocurrent density was attributed to reduction in Cu_{Zn} and grain growth induced by the partial substitution. A significantly positive onset of photocurrent would be derived from lowering VBM energy, leading to an increase in built-in potential.

Substitution of Sn^{4+} in a CZTS thin film was also studied for its PEC applications. Wen et al. demonstrated significant improvements in thin film quality, i.e., appreciable grain growth, achieved by partial substitution of Sn^{4+} with Ge^{4+} (CZGTS), resulting in improvement in photocurrent density at 0 V_{RHE} (11.1 mA·cm^{-2}) [95]. We found the effectiveness of Ge^{4+} replacement to induce an upward shift of the energy of the CBM; the photocathode based on the film with complete replacement of Ge^{4+} (CZGS) resulted in showing CO_2 reduction ability after applying surface modification of the ZnS layer [96]. Although functions of the surface coverage with ZnS have not yet been fully clarified, the modification might result in modulation of band alignment, passivation of interfacial defects, and creation of efficient catalytic sites for CO_2 reduction, leading to a ca. five times larger rate of CO evolution than that when using a CZGS thin film without any modification (Figure 13).

7 Further developments of photocathodic properties

Although the abovementioned recent reports show a rapid increase in PEC properties of copper kesterite compounds for water reduction, further improvements are required to reach a necessary level for predicting its practical use. Regarding the improvement of bulk properties of the kesterite thin film, extending the above-discussed

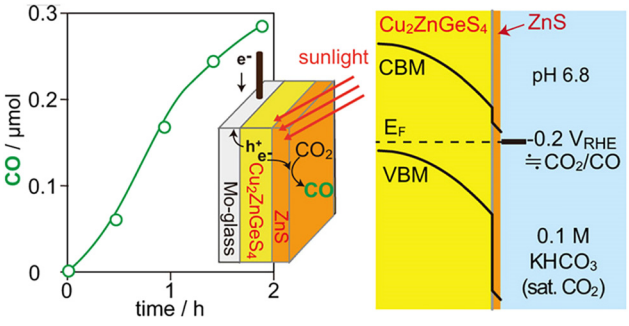

Figure 13: Time course curves of CO liberation over a ZnS/CZGS photocathode (left) and an estimated band alignment profile at the solid-liquid interface for the photocathode with application of a potential at −0.2 V_{RHE} (right). Reprinted with permission from ref. [96]. ©2019 American Chemical Society.

substitution concept to dual substitution would be worthy to be investigated. Indeed, Hadke et al. realized a kesterite-thin-film-based solar cell with sunlight conversion efficiency of 10.1% by applying partial substitutions of Cu and Zn sites in CZTS with Ag and Cd ($Cu_{1.8}Ag_{0.1}Cd_{0.3}Zn_{0.7}SnS_4$), respectively, the efficiency value of which was higher than that of a solar cell based on a kesterite thin film with 30% of Zn site substituted with Cd [97]. They suggested that the Cd substitution is likely to improve bulk properties of the kesterite thin film, leading to increase in carrier mobility and lifetime, whereas Ag substitution mainly contributes to improvements in interface quality of the kesterite n-type buffer layer (CdS) heterojunction, resulting in an increase in V_{OC}. Moreover, in view of band engineering, substitution of constituent elements in CZTS can also lead to modulate the E_g of CZTS. Therefore, band gap gradings also attempted to improve PEC properties of kesterite-based photocathodes. As has been proved by copper chalcopyrite Cu(In,Ga)Se_2-based solar cells [98], fabricating a V-shape grading of CBM would lead to improvements in saturated current density, photocurrent onset potential, and maximum HC-STH.

Another promising approach for improvements of PEC photocathodic properties is doping(s) of alkaline metal cations in the kesterite lattice. In the Cu(In,Ga)Se_2 solar cell technology, sodium (Na) doping is known to be indispensable to achieve a high efficiency, though the influence of Na-doping is still a debated topic [99]. Moreover, a potassium (K) treatment was found to be effective for further improvement of sunlight conversion efficiency of the Cu(In,Ga)Se2 solar cell [100]. Although the impact of the K-doping is also fully understand, critical properties affected by the K-doping are changes in chemical composition of the Cu(In,Ga)Se_2 layer and interface properties of the Cu(In,Ga)Se_2-CdS heterojunction. Regarding the copper kesterite-based solar cell, Li et al. reported that the Na doping in co-evaporated CZTSe thin film induced increase in the hole density as well as making the acceptor energy shallower, leading to enlargement of built-in potential to improve V_{OC} of the solar cell based on the Na-doped CZTSe thin film. The doped Na in the CZTSe thin film was also considered to reduce deep recombination centers in the kesterite, leading to further increase in V_{OC} of the solar cell. Thus, we can expect further improvements in PEC properties by applying appropriate loadings of alkaline components.

8 Conclusion

Copper kesterite CZTS is a promising candidate for a photocathode material for PEC water splitting because of its cost effectiveness and less toxicity of constituent

elements, appropriate photoabsorption properties, usability in the polycrystalline state, and chemical stability. Recent reports have shown rapid increases in the photocurrent density and onset potential of the photocurrent. One of the critical issues of these non-oxide-based PEC devices is its durability under operating conditions. Several works suggested the effectiveness of the use of a protection layer that is resistant to oxidative corrosion of surface-loaded components of the photocathode, such as CdS, leading to maximum stability up to several days for the continuous use of bias-free overall water splitting in a Z-scheme (tandem) system. The other important problem of the CZTS material is its point defect nature. To solve that problem, substitutions of constituent elements in the CZTS lattice were hypothesized: a novel defect engineering concept could be achieved by the replacement of Zn^{2+} with Cd^{2+} and Ba^{2+} as well as by replacement of Cu^{+} with Ag^{+}. Moreover, the concept of cation substitution also led to alterations of CBM and VBM energies of CZTS, resulting in improvements of PEC H_2 evolution property (especially photocurrent onset) as well as expression of CO_2 reduction ability. Although the PEC properties that have so far been achieved have not reached the necessary level for practical use, there is room for further development of PEC properties by using effective combinations among surface protection(s), defect engineering(s), and band engineering(s).

Acknowledgments: This work was supported by JSPS Grants-in-Aid for Scientific Research (KAKENHI), awards no. 19H02822, 20H05120, and 21K19033.

Funding information: JSPS Grants-in-Aid for Scientific Research (KAKENHI), awards no. 19H02822. JSPS Grants-in-Aid for Scientific Research (KAKENHI), awards no. 20H05120. JSPS Grants-in-Aid for Scientific Research (KAKENHI), awards no. 21K19033.

Author contributions: Shigeru Ikeda: conceptualization, writing – original draft, and writing – review and editing.

Conflict of interest: There is no conflict of interest.

References

[1] International Energy Agency (IEA). Key World Energy Statistics 2021: Supply, https://www.iea.org/reports/key-world-energy-statistics-2021/supply.

[2] International Energy Agency Photovoltaic Power Systems Programme (IEA PVPS). Snapshot of Global PV Markets 2021, https://iea-pvps.org/snapshot-reports/snapshot-2021/.

[3] Clegg, S. and P. Mancarella. Integrated modeling and assessment of the operational impact of power-to-gas (P2G) on electrical and gas transmission networks. *IEEE Transactions on Sustainable Energy*, Vol. 6, 2015, pp. 1234–1244.

[4] Møller, K. T., T. R. Jensen, E. Akiba, and H. Li. Hydrogen – a sustainable energy carrier. *Progress in Natural Science: Materials International*, Vol. 27, 2017, pp. 34–40.

[5] Rodriguez, C. A., M. A. Modestino, D. Psaltis, and C. Moser. Design and cost considerations for practical solar-hydrogen generators. *Energy & Environmental Science*, Vol. 7, 2014, pp. 3828–3835.

[6] Pinaud, B. A., J. D. Benck, L. C. Seitz, A. J. Forman, Z. Chen, T. G. Deutsch, et al. Technical and economic feasibility of centralized facilities for solar hydrogen production *via* photocatalysis and photoelectrochemistry. *Energy & Environmental Science*, Vol. 6, 2013, pp. 1983–2002.

[7] Hisatomi, T., T. Yamamoto, Q. Wang, T. Nakanishi, T. Higashi, M. Katayama, et al. Particulate photocatalyst sheets based on non-oxide semiconductor materials for water splitting under visible light irradiation. *Catalysis Science & Technology*, Vol. 8, 2018, pp. 3918–3925.

[8] Domen, K., A. Kudo, T. Onishi, N. Kosugi, and H. Kuroda. Photocatalytic decomposition of water into hydrogen and oxygen over nickel(II) oxide-strontium titanate ($SrTiO_3$) powder. 1. Structure of the catalysts. *The Journal of Physical Chemistry*, Vol. 90, No. 90, 1986, pp. 292–295.

[9] Maeda, K., K. Teramura, D. Lu, T. Takata, N. Saito, Y. Inoue, et al. Photocatalyst releasing hydrogen from water. *Nature*, Vol. 440, 2006, id. 295.

[10] Pan, C., T. Takata, M. Nakabayashi, T. Matsumoto, N. Shibata, Y. Ikuhara, et al. A complex perovskite-type oxynitride: the first photocatalyst for water splitting operable at up to 600 nm. *Angewandte Chemie International Edition*, Vol. 54, No. 54, 2015, pp. 2955–2959.

[11] Wang, Q., M. Nakabayashi, T. Hisatomi, S. Sun, S. Akiyama, Z. Wang, et al. Oxysulfide photocatalyst for visible-light-driven overall water splitting. *Nature Materials*, Vol. 18, 2019, pp. 827–832.

[12] Abe, R., K. Sayama, and H. Sugihara. Development of new photocatalytic water splitting into H_2 and O_2 using two different semiconductor photocatalysts and a shuttle redox mediator IO_3^-/I^-. *The Journal of Physical Chemistry B*, Vol. 109, 2005, pp. 16052–16061.

[13] Abe, R. Recent progress on photocatalytic and photoelectrochemical water splitting under visible light irradiation. *Journal of Photochemistry and Photobiology C: Photochemistry Reviews*, Vol. 11, 2010, pp. 179–209.

[14] Iwase, A., Y. H. Ng, Y. Ishiguro, A. Kudo, and R. Amal. Reduced graphene oxide as a solid-state electron mediator in z-scheme photocatalytic water splitting under visible light. *Journal of the American Chemical Society*, Vol. 133, 2011, pp. 11054–11057.

[15] Wang, Y., H. Suzuki, J. Xie, O. Tomita, D. J. Martin, M. Higashi, et al. Mimicking natural photosynthesis: solar to renewable H_2 fuel synthesis by z-scheme water splitting systems. *Chemical Reviews*, Vol. 118, 2018, pp. 5201–5241.

[16] Wang, Q., T. Hisatomi, Y. Suzuki, Z. Pan, J. Seo, M. Katayama, et al. Particulate photocatalyst sheets based on carbon conductor layer for efficient z-scheme pure-water splitting at

ambient pressure. *Journal of the American Chemical Society*, Vol. 139, 2017, pp. 1675–1683.
[17] Ockwig, N. W. and T. M. Nenoff. Membranes for hydrogen separation. *Chemical Reviews*, Vol. 107, 2007, pp. 4078–4110.
[18] Walter, M. G., E. L. Warren, J. R. McKone, S. W. Boettcher, Q. Mi, E. A. Santori, et al. Solar water splitting cells. *Chemical Reviews*, Vol. 110, 2010, pp. 6446–6473.
[19] Hisatomi, T., J. Kubota, and K. Domen. Recent advances in semiconductors for photocatalytic and photoelectrochemical water splitting. *Chemical Society Reviews*, Vol. 43, 2014, pp. 7520–7535.
[20] Zhang, K., M. Ma, P. Li, D. H. Wang, and J. H. Park. Water splitting progress in tandem devices: moving photolysis beyond electrolysis. *Advanced Energy Materials*, Vol. 6, 2016, id. 1600602.
[21] Yokoyama, D., T. Minegishi, K. Maeda, M. Katayama, J. Kubota, A. Yamada, et al. Photoelectrochemical water splitting using a Cu(In,Ga)Se_2 thin film. *Electrochemistry Communications*, Vol. 12, 2010, pp. 851–853.
[22] Ikeda, S., T. Nakamura, S. M. Lee, T. Yagi, T. Harada, T. Minegishi, et al. Photoreduction of water using modified $CuInS_2$ electrodes. *ChemSusChem*, Vol. 4, 2011, pp. 262–268.
[23] Moriya, M., T. Minegishi, H. Kumagai, M. Katayama, J. Kubota, and K. Domen. Stable hydrogen evolution from CdS-modified $CuGaSe_2$ photoelectrode under visible-light irradiation. *Journal of the American Chemical Society*, Vol. 135, 2013, pp. 3733–3735.
[24] Gunawan, W. Septina, S. Ikeda, T. Harada, T. Minegishi, K. Domen, et al. Platinum- and indium sulfide-modified $CuInS_2$ as efficient photocathodes for photoelectrochemical water splitting. *Chemical Communications*, Vol. 50, 2014, pp. 8941–8943.
[25] Kumagai, H., T. Minegishi, Y. Moriya, J. Kubota, and K. Domen. Photoelectrochemical hydrogen evolution from water using copper gallium selenide electrodes prepared by a particle transfer method. *The Journal of Physical Chemistry C*, Vol. 118, 2014, pp. 16386–16392.
[26] Mali, M. G., H. Yoon, B. N. Joshi, H. Park, S. S. Al-Deyab, D. C. Lim, et al. Enhanced photoelectrochemical solar water splitting using a platinum decorated CIGS/CdS/ZnO photocathode. *ACS Applied Materials & Interfaces*, Vol. 7, 2015, pp. 21619–21625.
[27] Zhao, J., T. Minegishi, L. Zhang, M. Zhong, Gunawan, M. Nakabayashi, et al. Enhancement of solar hydrogen evolution from water by surface modification with CdS and TiO_2 on porous $CuInS_2$ photocathodes prepared by an electrodeposition-sulfurization method. *Angewandte Chemie International Edition*, Vol. 53, No. 53, 2014, pp. 11808–11812.
[28] Septina, W., Gunawan, S. Ikeda, T. Harada, T. Higashi, R. Abe, et al. Photosplitting of water from wide-gap Cu(In,Ga)S_2 thin films modified with a CdS layer and Pt nanoparticles for a high-onset potential photocathode. *The Journal of Physical Chemistry C*, Vol. 119, 2015, pp. 8576–8583.
[29] Gunawan, W. Septina, T. Harada, Y. Nose, and S. Ikeda. Investigation of the electric structures of heterointerfaces in Pt- and In_2S_3-modified $CuInS_2$ photocathodes used for sunlight-induced hydrogen evolution. *ACS Applied Materials & Interfaces*, Vol. 7, 2015, pp. 16086–16092.
[30] Kaneko, H., T. Minegishi, M. Nakabayashi, N. Shibata, Y. Kuang, T. Yamada, et al. A novel photocathode material for sunlight-driven overall water splitting: solid solution of ZnSe and Cu(In,Ga)Se_2. *Advanced Functional Materials*, Vol. 26, 2016, pp. 4570–4577.
[31] Guijarro, N. M., S. Prévot, X. Yu, X. A. Jeanbourquin, P. Bornoz, W. Bourée, et al. A bottom-up approach toward all-solution-processed high-efficiency Cu(In,Ga)S_2 photocathodes for solar water splitting. *Advanced Energy Materials*, Vol. 6, 2016, id. 1501949.
[32] Septina, W., M. Sugimoto, D. Chao, Q. Shen, S. Nakatsuka, Y. Nose, et al. Photoelectrochemical water reduction over Ag-alloyed wide gap Cu(In,Ga)S_2 thin film photocathodes. *Physical Chemistry Chemical Physics*, Vol. 19, 2017, pp. 12502–12508.
[33] DeAngelis, A. D., K. Horsley, and N. Gaillard. Wide band gap $CuGa(S,Se)_2$ thin films on transparent conductive fluorinated tin oxide substrates as photocathode candidates for tandem water splitting devices. *The Journal of Physical Chemistry C*, Vol. 122, 2018, pp. 14304–14312.
[34] Kobayashi, H., N. Sato, M. Orita, Y. Kuang, H. Kaneko, T. Minegishi, et al. Development of highly efficient $CuIn_{0.5}Ga_{0.5}Se_2$-based photocathode and application to overall solar driven water splitting. *Energy & Environmental Science*, Vol. 11, 2018, pp. 3003–3009.
[35] Chen, M., Y. Liu, C. Li, A. Li, X. Chang, W. Liu, et al. Spatial control of cocatalysts and elimination of interfacial defects towards efficient and robust CIGS photocathodes for solar water splitting. *Energy & Environmental Science*, Vol. 11, 2018, pp. 2025–2034.
[36] Kim, B., G. S. Park, Y. J. Hwang, D. H. Won, W. Kim, D. K. Lee, et al. Cu(In,Ga)$(S,Se)_2$ photocathodes with a grown-in Cu_xS catalyst for solar water splitting. *ACS Energy Letters*, Vol. 4, 2019, pp. 2937–2944.
[37] Ikeda, S., W. Fujita, R. Okamoto, Y. Nose, R. Katsube, K. Yoshino, et al. Preparation of a $CuGaSe_2$ single crystal and its photocathodic properties. *RSC Advances*, Vol. 10, 2020, pp. 40310–40315.
[38] Ikeda, S., R. Okamoto, and S. Ishizuka. Enhancement of the photoelectrochemical properties of a $CuGaSe_2$-based photocathode for water reduction induced by loading of a Cu-deficient layer at the p–n heterointerface. *Applied Physics Letters*, Vol. 119, 2021, id. 083902.
[39] Paier, J., R. Asahi, A. Nagoya, and G. Kresse. Cu_2ZnSnS_4 as a potential photovoltaic material: a hybrid Hartree-Fock density functional theory study. *Physical Review B*, Vol. 79, 2009, id. 115126.
[40] Hall, S. R., J. T. Szymanski, and J. W. Stewart. Kesterite, $Cu_2(Zn,Fe)SnS_4$, and stannite, $Cu_2(Fe,Zn)SnS_4$, structurally similar but distinct minerals. *Canadian Mineralogist*, Vol. 16, 1978, pp. 131–137.
[41] Schorr, S. The crystal structure of kesterite type compounds: a neutron and X-ray diffraction study. *Solar Energy Materials & Solar Cells*, Vol. 95, 2011, pp. 1482–1488.
[42] Chen, S., X. G. Gong, A. Walsh, and S.-H. Wei. Crystal and electronic band structure of Cu_2ZnSnX_4 (X = S and Se) photovoltaic absorbers: first-principles insights. *Applied Physics Letters*, Vol. 94, 2009, id. 041903.
[43] Todorov, T. K., K. B. Reuter, and D. B. Mitzi. High-efficiency solar cell with earth-abundant liquid-processed absorber. *Advanced Materials*, Vol. 22, 2010, pp. E156–E159.
[44] Yang, W., H. S. Duan, B. Bob, H. Zhou, B. Lei, C. H. Chung, et al. Novel solution processing of high-efficiency earth-

abundant $Cu_2ZnSn(S, Se)_4$ solar cells. *Advanced Materials*, Vol. 24, 2012, pp. 6323–6329.

[45] Wang, W., M. T. Winkler, O. Gunawan, T. Gokmen, T. K. Todorov, Y. Zhu, et al. Device characteristics of CZTSSe thin-film solar cells with 12.6% efficiency. *Advanced Energy Materials*, Vol. 4, 2014, id. 1301465.

[46] Xin, H., K. J. Katahara, L. I. Braly, and W. H. Hillhouse. 8% efficient $Cu_2ZnSn(S, Se)_4$ solar cells from redox equilibrated simple precursors in DMSO. *Advanced Energy Materials*, Vol. 4, 2014, id. 1301823.

[47] Fu, J., J. Fu, Q. Tian, H. Wang, F. Zhao, J. Kong, et al. Tuning the Se content in $Cu_2ZnSn(S,Se)_4$ absorber to achieve 9.7% solar cell efficiency from a thiol/amine-based solution process. *ACS Applied Energy Materials*, Vol. 1, 2018, pp. 594–601.

[48] Gong, Y., Y. Zhang, Q. Zhu, Y. Zhou, R. Qiu, C. Niu, et al. Identify the origin of the V_{OC} deficit of kesterite solar cells from the two grain growth mechanisms induced by Sn^{2+} and Sn^{4+} precursors in DMSO solution. *Energy & Environmental Science*, Vol. 14, 2021, pp. 2369–2380.

[49] Persson, C. Electronic and optical properties of Cu_2ZnSnS_4 and $Cu_2ZnSnSe_4$. *Journal of Applied Physics*, Vol. 107, 2010, id. 053710.

[50] Haight, R., A. Barkhouse, O. Gunawan, B. Shin, M. Copel, M. Hopstaken, et al. Band alignment at the $Cu_2ZnSn(S_xSe_{1-x})_4$/CdS interface. *Applied Physics Letters*, Vol. 98, 2011, id. 253502.

[51] Ito, K. and T. Nakazawa. Electrical and optical properties of stannite-type quaternary semiconductor thin films. *Japanese Journal of Applied Physics*, Vol. 27, 1988, pp. 2094–2097.

[52] Metzner, H. and T. Hahn. Sulphur-terminated silicon surfaces for the epitaxial growth of chalcopyrite semiconductors. *Journal of Crystal Growth*, Vol. 225, 2001, pp. 354–358.

[53] Olekseyuk, I. D., I. V. Dudchak, and L. V. Piskach. Phase equilibria in the Cu_2S–ZnS–SnS_2 system. *Journal of Alloys and Compounds*, Vol. 368, 2004, pp. 135–143.

[54] Du, H., F. Yan, M. Young, B. To, C.-S. Jiang, P. Dippo, et al. Investigation of combinatorial coevaporated thin film Cu_2ZnSnS_4. I. Temperature effect, crystalline phases, morphology, and photoluminescence. *Journal of Applied Physics*, Vol. 115, 2014, id. 173502.

[55] Kumar, M., A. Dubey, N. Adhikari, S. Venkatesan, and Q. Qiao. Strategic review of secondary phases, defects and defect-complexes in kesterite CZTS-Se solar cell. *Energy & Environmental Science*, Vol. 8, 2015, pp. 3134–3159.

[56] Umehara, M., Y. Takeda, T. Motohiro, T. Sakai, H. Awano, and R. Maekawa. $Cu_2Sn_{1-x}Ge_xS_3$ (x = 0.17) thin-film solar cells with high conversion efficiency of 6.0%. *Applied Physics Express*, Vol. 6, 2013, id. 045501.

[57] Liu, F., S. Hu, X. Ding, J. Zhu, J. Wen, X. Pan, et al. Ligand-free nano-grain Cu_2SnS_3 as a potential cathode alternative for both cobalt and iodine redox electrolyte dye-sensitized solar cells. *Journal of Materials Chemistry A*, Vol. 4, 2016, pp. 14865–14876.

[58] Burton, L. A., D. Colombara, R. D. Abellon, F. C. Grozema, L. M. Peter, T. J. Savenije, et al. Synthesis, characterization, and electronic structure of single-crystal SnS, Sn_2S_3, and SnS_2. *Chemistry of Materials*, Vol. 25, 2013, pp. 4908–4916.

[59] Chen, S., J.-H. Yang, X. G. Gong, A. Walsh, and S.-H. Wei. Intrinsic point defects and complexes in the quaternary kesterite semiconductor Cu_2ZnSnS_4. *Physical Review B*, Vol. 81, 2010, id. 245204.

[60] Chen, S., A. Walsh, X. G. Gong, and S. H. Wei. Classification of lattice defects in the kesterite Cu_2ZnSnS_4 and $Cu_2ZnSnSe_4$ earth-abundant solar cell absorbers. *Advanced Materials*, Vol. 25, 2013, pp. 1522–1539.

[61] Zhang, S. B., S.-H. Wei, A. Zunger, and H. Katayama-Yoshida. Defect physics of the $CuInSe_2$ chalcopyrite semiconductor. *Physical Review B*, Vol. 57, 1998, id. 9642.

[62] Wei, S.-H. and S. B. Zhang. Defect properties of $CuInSe_2$ and $CuGaSe_2$. *Journal of Physics and Chemistry of Solids*, Vol. 66, 2005, pp. 1994–1999.

[63] Nagaoka, A., K. Yoshino, H. Taniguchi, T. Taniyama, and H. Miyake. Preparation of Cu_2ZnSnS_4 single crystals from Sn solutions. *Journal of Crystal Growth*, Vol. 341, 2012, pp. 38–41.

[64] Nagaoka, A., H. Miyake, T. Taniyama, K. Kakimoto, and K. Yoshino. Correlation between intrinsic defects and electrical properties in the high-quality Cu_2ZnSnS_4 single crystal. *Applied Physics Letters*, Vol. 103, 2013, id. 112107.

[65] Bourdais, S., C. Choné, B. Delatouche, A. Jacob, G. Larramona, C. Moisan, et al. Is the Cu/Zn disorder the main culprit for the voltage deficit in kesterite solar cells? *Advanced Energy Materials*, Vol. 6, 2016, id. 1502276.

[66] Yin, L., G. Cheng, Y. Feng, Z. Li, C. Yang, and X. Xiao. Limitation factors for the performance of kesterite Cu_2ZnSnS_4 thin film solar cells studied by defect characterization. *RSC Advances*, Vol. 5, 2015, pp. 40369–40374.

[67] Qi, Y.-F., D.-X. Kou, W.-H. Zhou, Z.-J. Zhou, Q.-W. Tian, Y.-N. Meng, et al. Engineering of interface band bending and defects elimination *via* a Ag-graded active layer for efficient $(Cu,Ag)_2ZnSn(S,Se)_4$ solar cells. *Energy & Environmental Science*, Vol. 10, 2017, pp. 2401–2410.

[68] Katagiri, H., M. Nishimura, T. Onozawa, S. Maruyama, M. Fujita, T. Sega, et al. Rare-metal free thin film solar cell. *Proceeding of the Power Conversion Conference*, Vol. 2, 1997, pp. 1003–1006.

[69] Friedlmeier, M., N. Wieser, and T. Walter. Heterojunctions based on Cu_2ZnSnS_4 and $Cu_2ZnSnSe_4$ thin films. *Proceeding of the 14th Eur PVSEC Exhibition*, 1997, pp. 10–13.

[70] Katagiri, H., K. Jimbo, W. S. Maw, K. Oishi, M. Yamazaki, A. Araki, et al. Development of CZTS-based thin film solar cells. *Thin Solid Films*, Vol. 517, 2009, pp. 2455–2460.

[71] Katagiri, H., K. Jimbo, S. Yamada, T. Kamimura, W. S. Maw, T. Fukano, et al. Enhanced conversion efficiencies of Cu_2ZnSnS_4-based thin film solar cells by using preferential etching technique. *Applied Physics Express*, Vol. 1, 2008, id. 041201.

[72] Yan, C., K. Sun, J. Huang, S. Johnston, F. Liu, B. P. Veettil, et al. Beyond 11% efficient sulfide kesterite $Cu_2Zn_xCd_{1-x}SnS_4$ solar cell: effects of cadmium alloying. *ACS Energy Letters*, Vol. 2, 2017, pp. 930–936.

[73] Minemoto, T., T. Matsui, H. Takakura, Y. Hamakawa, T. Negami, Y. Hashimoto, et al. Theoretical analysis of the effect of conduction band offset of window/CIS layers on performance of CIS solar cells using device simulation. *Solar Energy Materials and Solar Cells*, Vol. 67, 2001, pp. 83–88.

[74] Yokoyama, D., T. Minegishi, K. Jimbo, T. Hisatomi, G. Ma, M. Katayama, et al. H_2 evolution from water on modified Cu_2ZnSnS_4 photoelectrode under solar light. *Applied Physics Express*, Vol. 3, 2010, id. 101202.

[75] Yang, W., Y. Oh, J. Kim, M. J. Jeong, J. H. Park, and J. Moon. Molecular chemistry controlled hybrid ink-derived efficient

Cu_2ZnSnS_4 photocathodes for photoelectrochemical water splitting. *ACS Energy Letters*, Vol. 1, 2016, pp. 1127–1136.

[76] Jiang, F., T. Harada, Y. Kuang, T. Minegishi, K. Domen, et al. $Pt/In_2S_3/CdS/Cu_2ZnSnS_4$ thin film as an efficient and stable photocathode for water reduction under sunlight radiation. *Journal of the American Chemical Society*, Vol. 137, 2015, pp. 13691–13697.

[77] Huang, D., K. Wang, L. Yu, T. H. Nguyen, S. Ikeda, S. F. Jiang, et al. Over 1% efficient unbiased stable solar water splitting based on a sprayed Cu_2ZnSnS_4 photocathode protected by a HfO_2 photocorrosion-resistant film. *ACS Energy Letters*, Vol. 3, 2018, pp. 1875–1881.

[78] Wang, K., D. Huang, L. Yu, H. Gu, S. Ikeda, and F. Jiang. Environmentally friendly Cu_2ZnSnS_4-based photocathode modified with a ZnS protection layer for efficient solar water splitting. *Journal of Colloid and Interface Science*, Vol. 536, 2019, pp. 9–16.

[79] Huang, D., K. Wang, L. Li, K. Feng, N. An, S. Ikeda, et al. 3.17% efficient Cu_2ZnSnS_4-$BiVO_4$ integrated tandem cell for standalone overall solar water splitting. *Energy & Environmental Science*, Vol. 14, 2021, pp. 1480–1489.

[80] Tay, Y. F., H. Kaneko, S. Y. Chiam, S. Lie, Q. Zheng, B. Wu, et al. Solution-processed Cd-substituted CZTS photocathode for efficient solar hydrogen evolution from neutral water. *Joule*, Vol. 2, 2018, pp. 537–548.

[81] Ge, J., Y. Yu, and Y. Yan. Earth-abundant trigonal $BaCu_2Sn(Se_xS_{1-x})_4$ (x = 0–0.55) thin films with tunable band gaps for solar water splitting. *Journal Materials Chemistry A*, Vol. 4, 2016, pp. 18885–18891.

[82] Shin, D., E. Ngaboyamahina, Y. Zhou, J. T. Glass, and D. B. Mitzi. Synthesis and characterization of an earth-abundant $Cu_2BaSn(S,Se)_4$ chalcogenide for photoelectrochemical cell application. *The Journal of Physical Chemistry Letters*, Vol. 7, 2016, pp. 4554–4561.

[83] Ge, J., P. J. Roland, P. Koirala, W. Meng, J. L. Young, R. Petersen, et al. Employing overlayers to improve the performance of Cu_2BaSnS_4 thin film based photoelectrochemical water reduction devices. *Chemistry of Materials*, Vol. 29, 2017, pp. 916–920.

[84] Zhou, Y., D. Shin, E. Ngaboyamahina, G. Han, C. B. Parker, and D. B. Mitzi. Efficient and stable $Pt/TiO_2/CdS/Cu_2BaSn(S,Se)_4$ photocathode for water electrolysis applications. *ACS Energy Letters*, Vol. 3, 2018, pp. 177–183.

[85] Shin, D., B. Saparov, T. Zhu, W. P. Huhn, V. Blum, and D. B. Mitzi. $BaCu_2Sn(S,Se)_4$: earth-abundant chalcogenides for thin-film photovoltaics. *Chemistry of Materials*, Vol. 28, 2016, pp. 4771–4780.

[86] Shin, D., T. Zhu, X. Huang, O. Gunawan, V. Blum, and D. B. Mitzi. Earth-abundant chalcogenide photovoltaic devices with over 5% efficiency based on a $Cu_2BaSn(S,Se)_4$ absorber. *Advanced Materials*, Vol. 29, 2017, id. 1606945.

[87] Yuan, Z. K., S. Chen, H. Xiang, X. G. Gong, A. Walsh, J. S. Park, et al. Engineering solar cell absorbers by exploring the band alignment and defect disparity: the case of Cu and Ag-based kesterite compounds. *Advanced Functional Materials*, Vol. 25, 2015, pp. 6733–6743.

[88] Nguyen, T. H., T. Kawaguchi, J. Chantana, T. Minemoto, T. Harada, S. Nakanishi, et al. Structural and solar cell properties of an Ag-containing Cu_2ZnSnS_4 thin film derived from spray pyrolysis. *ACS Applied Materials & Interfaces*, Vol. 10, 2018, pp. 5455–5463.

[89] Huang, W.-C., S.-Y. Wei, C.-H. Cai, W.-H. Ho, and C.-H. Lai. The role of Ag in aqueous solution processed $(Ag,Cu)_2ZnSn(S,Se)_4$ kesterite solar cells: antisite defect elimination and importance of Na passivation. *Journal of Materials Chemistry A*, Vol. 6, 2018, pp. 15170–15181.

[90] Qi, Y., Q. Tian, Y. Meng, D. Kou, Z. Zhou, W. Zhou, et al. Elemental precursor solution processed $(Cu_{1-x}Ag_x)_2ZnSn(S,Se)_4$ photovoltaic devices with over 10% efficiency. *ACS Applied Materials Interfaces*, Vol. 9, 2017, pp. 21243–21250.

[91] Xu, Z., Z. Guan, J. Yang, and G. Li. Band positions and photoelectrochemical properties of solution-processed silver-substituted Cu_2ZnSnS_4 photocathode. *ACS Applied Energy Materials*, Vol. 2, 2019, pp. 2779–2785.

[92] Tay, Y. F., S. S. Hadke, M. Zhang, N. Lim, S. Y. Chiamd, and L. H. Wong. Improving the interfacial properties of CZTS photocathodes by Ag substitution. *Journal of Materials Chemistry A*, Vol. 8, 2020, pp. 8862–8867.

[93] Ikeda, S., T. H. Nguyen, R. Okamoto, M. Remeika, I. Abdellaoui, M. M. Islam, et al. Effects of incorporation of Ag into a kesterite Cu_2ZnSnS_4 thin film on its photoelectrochemical properties for water reduction. *Physical Chemistry Chemical Physics*, 2022, Doi: 10.1039/D1CP04075H.

[94] Ikeda, S., T. Nakamura, T. Harada, and M. Matsumura. Multicomponent sulfides as narrow gap hydrogen liberation photocatalysts. *Physical Chemistry Chemical Physics*, Vol. 12, 2010, pp. 13943–13949.

[95] Wen, X., W. Luo, Z. Guan, W. Huang, and Z. Zou. Boosting efficiency and stability of a Cu_2ZnSnS_4 photocathode by alloying Ge and increasing sulfur pressure simultaneously. *Nano Energy*, Vol. 41, 2017, pp. 18–26.

[96] Ikeda, S., S. Fujikawa, T. Harada, T. H. Nguyen, S. Nakanishi, T. Takayama, et al. Photocathode characteristics of a spray-deposited Cu_2ZnGeS_4 thin film for CO_2 reduction in a CO_2-saturated aqueous solution. *ACS Applied Energy Materials*, Vol. 2, 2019, pp. 6911–6918.

[97] Hadke, S. H., S. Levcenko, S. Lie, C. J. Hages, J. A. Márquez, T. Unold, et al. Synergistic effects of double cation substitution in solution-processed CZTS solar cells with over 10% efficiency. *Advanced Energy Materials*, Vol. 8, 2018, id. 1802540.

[98] Repins, I., M. A. Contreras, B. Egaas, C. DeHart, J. Scharf, C. L. Perkins, et al. 19.9%-Efficient ZnO/CdS/$CuInGaSe_2$ solar cell with 81.2% fill factor. *Progress in Photovoltaics: Research and Applications*, Vol. 16, 2008, pp. 235–239.

[99] Niki, S., M. Contreras, I. Repins, M. Powalla, K. Kushiya, S. Ishizuka, et al. CIGS absorbers and processes. *Progress in Photovoltaics: Research and Applications*, Vol. 18, 2010, pp. 453–466.

[100] Chirilă, A., P. Reinhard, F. Pianezzi, P. Bloesch, A. R. Uhl, C. Fella, et al. Potassium-induced surface modification of Cu$(In,Ga)Se_2$ thin films for high-efficiency solar cells. *Nature Materials*, Vol. 12, 2013, pp. 1107–1111.